

Auxiliary Material

Long-term drought severity variations in Morocco

Jan Esper¹, David Frank¹, Ulf Büntgen¹, Anne Verstege¹, Jürg Luterbacher², Elena Xoplaki²

¹ Swiss Federal Research Institute WSL, Birmensdorf, Switzerland

² National Centre of Competence in Research on Climate (NCCR) and Institute of Geography, University of Bern, Bern, Switzerland.

1. *Cedrus atlantica* site chronologies

Ten RCS detrended site chronologies [Esper *et al.*, 2007b] were developed and grouped into six shorter (<500 years) and four longer (>500 years) records (Table S1, Figure S1). Cumulative replication of the short chronologies reaches a maximum of 138 series in the 1960s, but declines back in time, e.g., is 49 in 1800. Replication of the long chronologies is 312 in the 1950s, with substantial contributions from Col, and declines to 44 series in 1290 when the first site (Tou) falls below 5 series and drops out. Importantly, while only one of the shorter sites (Taa) has been updated to 2001, all of the long-term sites contain recent data from the 1990s. Cumulative replication of the old growth sites is 177 series in 2001. The expressed population signal (EPS, Wigley *et al.*, 1984) indicates that the mean chronologies of the short-term records are less representative of the theoretical population means in comparison to the long-term records (top of panels A and B in figure S1). Afe and Taa possess EPS values >0.85 back to 1805 and 1780, and Ifr back to 1605, respectively. The old growth sites, however, indicate strength back to 1330 (Tiz and Tou) and 1130 (Jaf and Col).

	Site	Lat./Lon.	Elevation (m asl.)	Period	Series/tree number	Mean series length (yrs.)	Tree-ring number	Cross correlation	Source
Rif Atlas	Tis	35°07'/5°06'	1'700	1748-1984	14/ 10	176	6'561	0.59	Stockton
	Afe	35°02'/4°50'	1'700	1632-1984	31/ 14	212	2'464	0.67	Stockton
E Middle Atlas	Taz	34°05'/4°11'	1'900	1845-1984	28/ 14	105	2'951	0.55	Stockton
	Iso	33°24'/5°10'	1'830	1784-2001	41/ 25	105	4'321	0.62	Esper
W Middle Atlas	Ifr	33°27'/5°02'	1'900	1549-1984	39/ 16	249	9'701	0.69	Stockton
	Tiz	33°06'/4°54'	2'180	987-2001	53/ 35	423	22'409	0.72	Esper
	Col	32°58'/5°04'	2'200	977-2001	144/ 72	365	52'499	0.71	Esper/Stockton
	Tou	32°25'/5°20'	2'100	1253-2001	77/ 39	409	31'451	0.71	Esper/Stockton
High Atlas	Jaf	32°32'/4°55'	2'200	1021-2001	52/ 32	536	27'835	0.83	Esper
	Taa	32°23'/5°36'	2'200	1728-1984	21/ 12	176	4'296	0.78	Stockton
	TCTJ			977-2001	326/178	412	134'194	0.63	
	TCTJ-1600			977-2001	174/110	577	100'340	0.63	
	TCTJ-1400			1177-2001	87/ 64	474	41'259	0.63	

Table S1. Characteristics of *Cedrus atlantica* site chronologies and merged files (TCTJ) combining data from Tiz, Col, Tou and Jaf.

While the short-term site chronologies share only little decadal scale variance – perhaps with the exception of the generally higher chronology values in the 1960s – the long-term records are characterized by high degrees of common variability (Figure S1 B). Most of the decadal scale fluctuations, including the rapid change to low chronology levels in the late 1970s, are common to all old growth site records. Moreover, the long-term records all indicate lower chronology levels before ~1350 – perhaps except for the highly variable but weakly replicated early Tou data – and generally higher levels after ~1450. This long-term change from persistently low to high chronology levels indicates substantial loading in the centennial scale frequency domain.

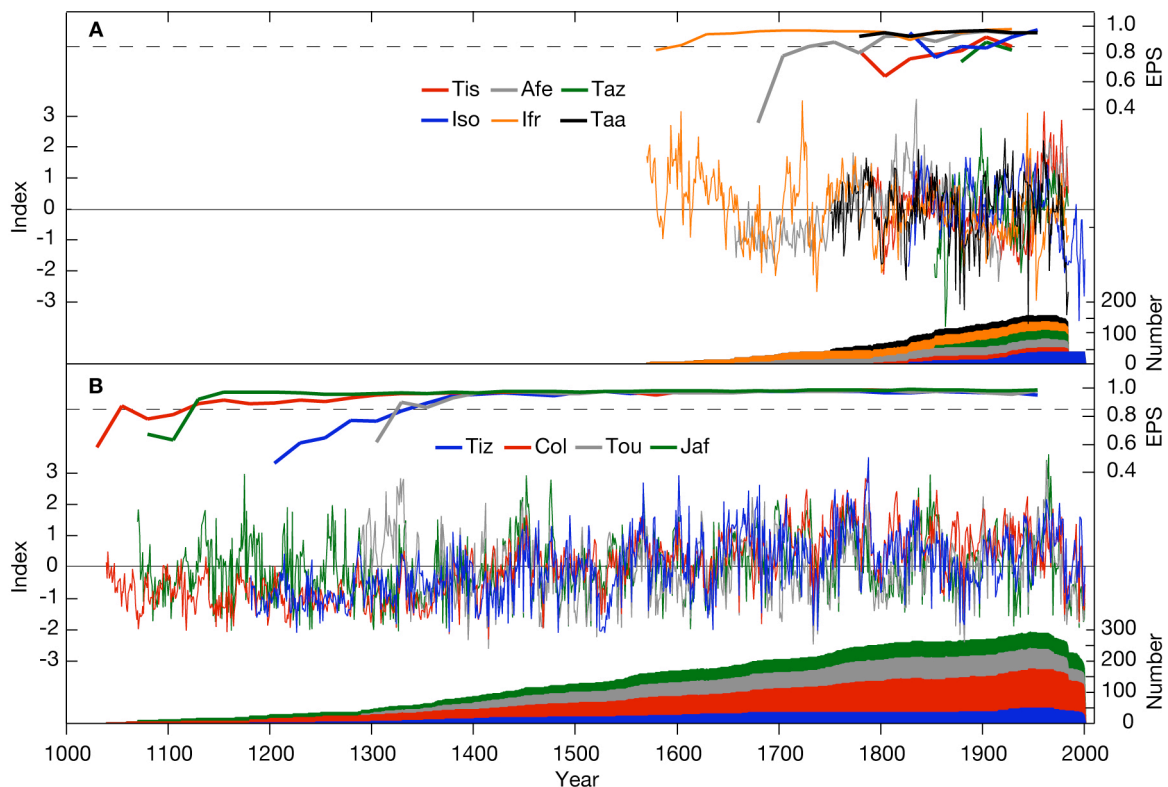


Figure S1. *Cedrus atlantica* short-term (A) and long-term (B) site chronologies. Colored bands specify the number of series averaged in a site chronology. Chronologies truncated at $n = 5$ series. Curves at the top show EPS calculated over 50-year segments lagged by 25 years. Dashed curves indicate $EPS = 0.85$.

Analysis of the coherence between site chronologies revealed high correlations between the geographically proximal sites in the Rif, Middle, and High Atlas (Figure 1) over the 1853-1984 and 1751-1984 periods (Table S2). Average correlation between all site records is 0.22, and 0.53 between the old growth sites Tiz, Col, Tou, and Jaf. Highly significant results are also obtained over the much longer 1290-2001 period using original ($r = 0.53$) and 20-year smoothed ($r = 0.47$) records.

		1853-1984										
		Tis	Afe	Taz	Iso	Ifr	Tiz	Col	Tou	Jaf	Taa	Mean
1751-1984	Tis*		0.71	0.17	-0.25	-0.03	0.28	-0.17	0.11	0.31	-0.06	0.11 Tis
	Afe	0.59		0.12	-0.17	0.12	0.26	-0.12	0.02	0.17	-0.11	0.12 Afe
	Taz*	0.17	0.12		-0.09	-0.12	-0.11	0.06	-0.05	-0.10	-0.16	-0.03 Taz
	Iso*	-0.22	-0.12	-0.09		0.27	0.26	0.51	0.41	0.26	0.47	0.19 Iso
	Ifr	0.02	0.22	-0.12	0.24		0.25	0.42	0.10	-0.02	0.20	0.18 Ifr
	Tiz	0.23	0.22	-0.11	0.27	0.43		0.42	0.65	0.59	0.59	0.36 Tiz
	Col	-0.13	0.03	0.06	0.48	0.56	0.60		0.47	0.26	0.52	0.30 Col
	Tou	0.09	-0.02	-0.05	0.39	0.24	0.60	0.52		0.69	0.76	0.35 Tou
	Jaf	0.28	0.13	-0.10	0.31	0.20	0.52	0.36	0.71		0.54	0.31 Jaf
	Taa	-0.05	-0.04	-0.16	0.44	0.30	0.53	0.53	0.70	0.48		0.30 Taa
0.22 All												
0.53 TCTJ												

		1290-2001 Annual			
		Tiz	Col	Tou	Jaf
20-yr. filter	Tiz		0.69	0.48	0.56
	Col	0.74		0.36	0.51
	Tou	0.31	0.16		0.58
	Jaf	0.56	0.57	0.49	

0.53 TCTJ
0.47 TCTJ

Table S2. Correlations between cedar site chronologies. Top: Results for the 1853-1984 common period, and the 1751-1984 period during which all except of three chronologies (*) have data. Right column lists the mean values for each site, for all data, and for the old growth sites Tiz, Col, Tou, and Jaf (TCTJ). Bottom: Results for the 1290-2001 period common to the TCTJ sites, using original and 20-year smoothed chronologies.

Common variance between the nearby site chronologies from Tiz, Col, Tou, and Jaf supported combination of the old growth data into a merged dataset TCTJ integrating 326 tree-ring series consisting of ~134,000 annual width measurements. For the purpose of exploring PDSI-related long-term trends, we also used subsets of TCTJ where we excluded trees younger than AD 1600 (TCTJ-1600) and even younger than 1400 (TCTJ-1400). However, these selections result in data reductions 100,000 and 41,000 ring width measurements, respectively (Table S1).

2. Detrending methods and low frequency characteristics

Low frequency spectra of millennium-long tree-ring records are explored by applying various detrending methods to the old growth ring width data combined in TCTJ, and in the TCTC-1600 and TCTC-1400 sub-samples (Table S1). Common to all these approaches is the application of a variance stabilization of the resulting chronologies that considers temporal changes in sample replication and

interseries correlation [Frank *et al.*, 2007], and the utilization of the arithmetic mean for chronology calculation. MTM power spectra [Mann and Lees, 1996] are used to analyze low frequency differences between chronologies.

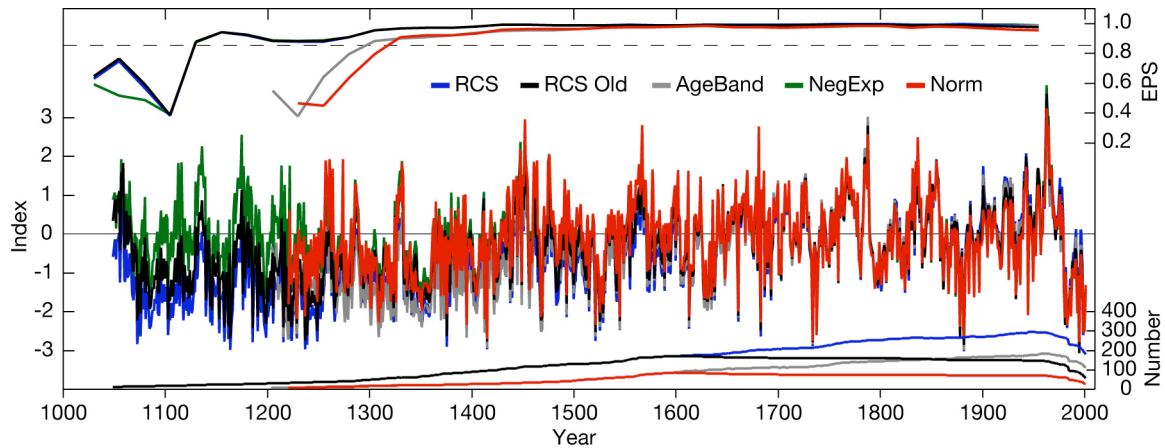


Figure S2. Five differently detrended chronologies using various sub-sets of the TCTJ tree-ring data. Curves at the top and bottom indicate EPS calculated over 50-year segments lagged by 25 years and the sample replication of chronologies.

Detrending approaches include:

- (i) Regional Curve Standardization (RCS) used with TCTJ [Esper *et al.*, 2003a]. The Regional Curve (RC) was designated using a 100-year spline, and the resulting record termed "RCS".
- (ii) RCS used with TCTJ-1600. This is the same approach as outlined in (i) but applied to the reduced TCTJ-1600 sub-sample, from which all measurement series shorter than AD 1600 have been removed. Resulting record is termed "RCS Old".
- (iii) Age Banding Method [Briffa *et al.*, 2001] considering a large band ranging from 200-650 years used with TCTJ. This method is similar to (i) except for the aspect that very young and very old, i.e. potentially more noisy, rings were removed from the analysis. Resulting record is termed "AgeBand".
- (iv) Individual negative exponential and straight line detrending used with TCTJ [Fritts, 1976]. Resulting record is termed "NegExp".
- (v) A regular normalization used with TCTJ-1400 [Esper *et al.*, 2003b]. This method comprises a z-transformation of the TCTJ-1400 sub-sample, from which both the measurement series younger than AD 1400 and the juvenile tree-rings younger than 200 years cambial age have been removed. Resulting record is termed "Norm".

These efforts were effectively made to assess the non-biological (i.e., climatic) component in the centennial scale trend from lower chronology levels before ~1350 to higher levels after ~1450, as seen in the old growth site chronologies. Comparison of the detrending methods demonstrated that NegExp revealed highest and RCS lowest chronology levels before ~1200 (Figure S2). RCS Old arrived in

between these two extremes in this early period of the past millennium. Due to the removal of young tree-rings in the Age Banding approach and the use of the truncated TCTJ-1400 data in the Norm approach, these records do not reach back to 1049, and allow comparisons only until 1204 and 1221, respectively. The EPS indicates reasonable signal strength back to about 1120 for RCS, RCS Old and NexExp, and back to 1300 and 1320 for AgeBand and Norm, respectively.

While generally larger chronology differences are evident during the earliest portion of the past millennium, the period between 1250 and 1360 is characterized by low variance between the long-term records. All chronologies portray low values before ~1360 and a long-term increase until ~1450, i.e. the differing detrendings and utilization of various sub-samples of TCTJ all support the low frequency change during the 14th and 15th centuries, as seen in the old growth site chronologies.

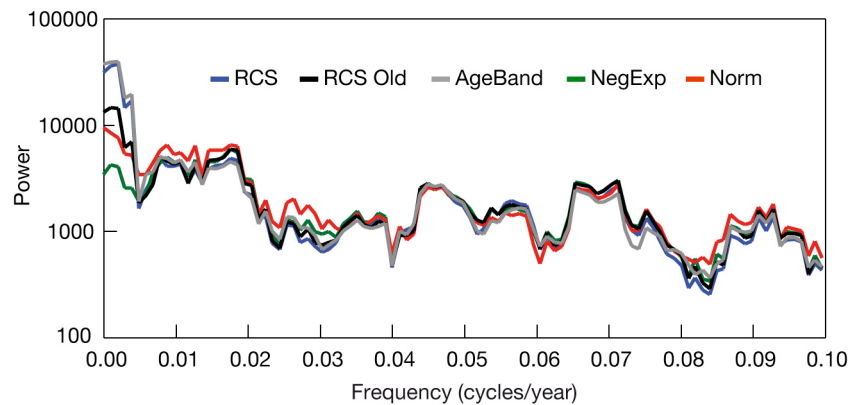


Figure S3. MTM spectra of five differently detrended TCTJ chronologies calculated over the 1121-2001 common period using 5-year resolution and 3 tapers.

Systematic differences between the five chronologies occur in the lowest frequency domain >200 years (Figure S3). While clearly reduced low frequency loading was, as expected [Esper *et al.*, 2002, 2004], found in the individually detrended NegExp record, RCS and AgeBand revealed highest such loading. Norm and RCS Old appear in between the other chronologies, suggesting that these records portray intermediate representations of the low frequency drought history in Morocco.

Importantly, all detrendings resulted in "useful" chronologies, i.e., they could have been utilized as the single best realization of common variance stored in cedar tree-rings over the past millennium (and published as this) [Esper *et al.*, 2007a]. Instead we use these different "reasonable possibilities" to help estimate a methodological uncertainty (see below). Differences between these records are limited to the lowest frequency domain, where statistical timeseries analyses are largely restricted due to reduced degrees of freedom [Cook *et al.*, 2004]. Consequently, calibration tests against instrumental PDSI and precipitation data do not reveal significant difference between the various chronologies.

3. Trend preservation via RCS

Analysis of the RCS method applied to all TCTJ data indicated that resulting chronologies contain increasing long-term trends that are possibly exaggerated by the inclusion of measurement series from younger trees. This potential bias has been assessed by splitting the TCTJ data into Young and Old sub-samples, integrating 152 tree-ring series <AD 1600 and 174 series >AD 1600, respectively. Alignment of these sub-samples by cambial age revealed substantial differences in initial growth rates and age trends (Figure S4). The Young data contain much wider rings (initially about 1.6 mm) and a steeper age trend than the Old data (first rings about 1.1 mm).

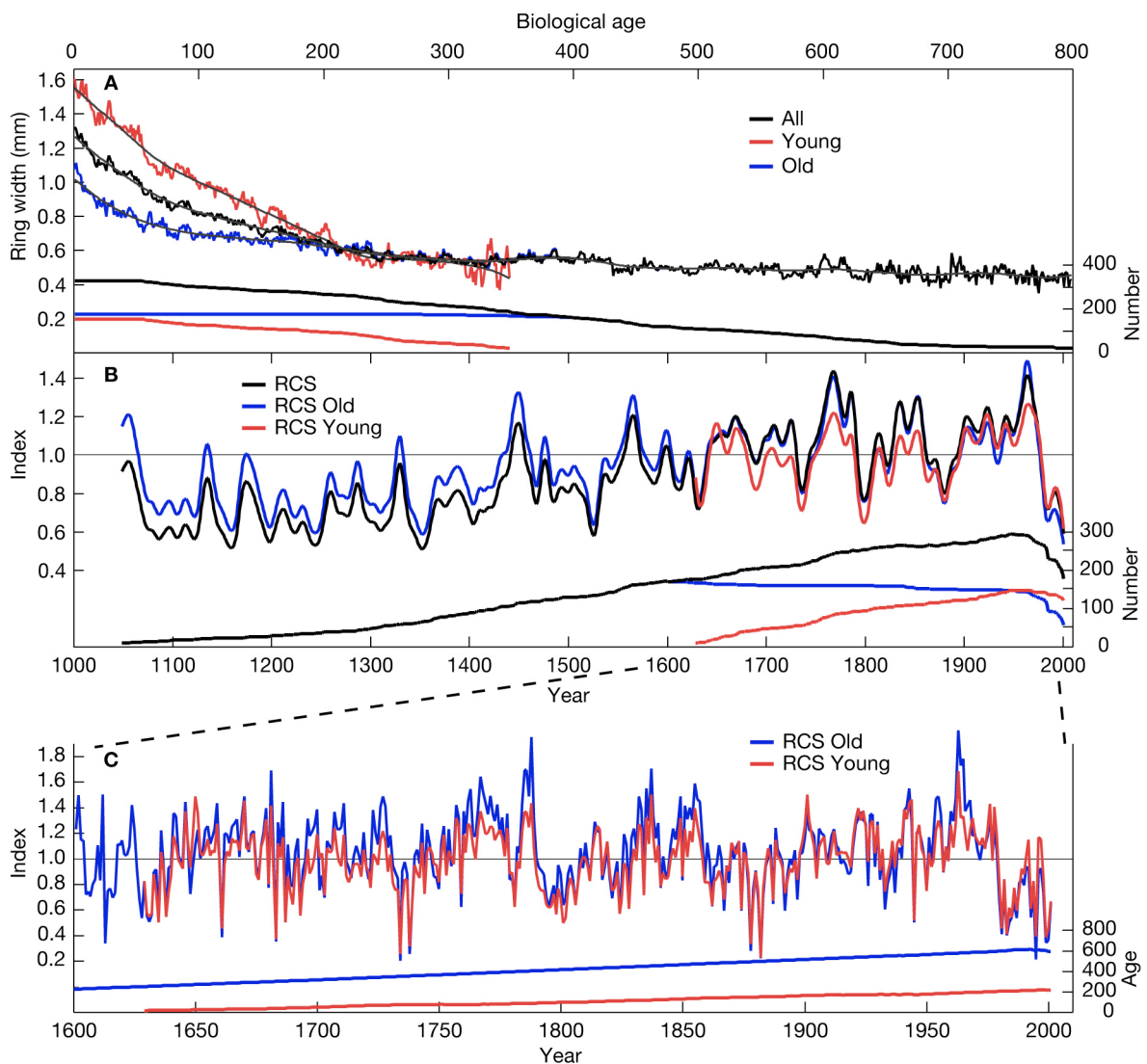


Figure S4. Effect of sample composition and age structure on the low and high frequency characteristics of RCS chronologies. (A) Arithmetic mean curves of the age-aligned TCTJ All, Young, and Old (= TCTJ-1600) ring width data. Smooth curves are the Regional Curves used for detrending in the RCS procedure. Curves at the bottom indicate sample replication. (B) 20-year smoothed RCS chronologies of the TCTJ All, Young, and

Old data. Sample replication at the bottom. (C) Annually resolved Old and Young RCS chronologies. Curves at bottom indicate the average age of tree-rings integrated in the chronologies.

These differences might to some extent arise from the tendency of greater pith offset (PO) – which is the difference in years between the innermost ring on a core sample and the true center or pith of a tree at sampling height – in larger trees [Esper *et al.*, 2006]. In other words, there is a tendency that more innermost tree-rings were missed on core samples from old trees than on samples from young trees. The key reason for this tendency is the sheer size of Moroccan cedar trees, with individuals frequently exceeding diameters of 4-5 m at breast height. As a consequence, differently old tree-rings are related to each other within the RCS procedure [Esper *et al.*, 2003a]. This is particularly important as the young trees, with greater growth values cover only the recent end of the chronology. And as such, they may impart a bias towards a positive trend in recent times.

This bias likely affected the RCS chronology integrating all TCTJ data, as the younger, post AD 1600, data fell more often above the RC from all data (the smooth curve fit to the data shown in black in Figure S4 A). However, while these tendencies might artificially increase the positive trend in the RCS chronology, the RCS Old chronology derived from using only the old, TCTJ-1600 data might suffer from the removal of young tree-rings, i.e. could potentially miss some climatically induced low frequency information. Our results though indicate that these effects are small (Figure S4 B), and favoring one of the records over the other is certainly not feasible at this point.

Comparison of the decadal scale and higher frequency variability between the RCS Young and Old chronologies demonstrated similarity of the information stored in differently old tree-rings (Figure S4 C). Correlation between these independent chronologies is 0.91 over the 1629-2001 period of overlap. The difference in mean chronology age increased from ~240 to 400 years over the same period. These results indicate the temporal robustness of our long-term proxy record, as young and old tree-rings effectively show parallel variability. That is they store the same environmental signals, which demonstrates any potential differences in the response of differently aged trees to be small.

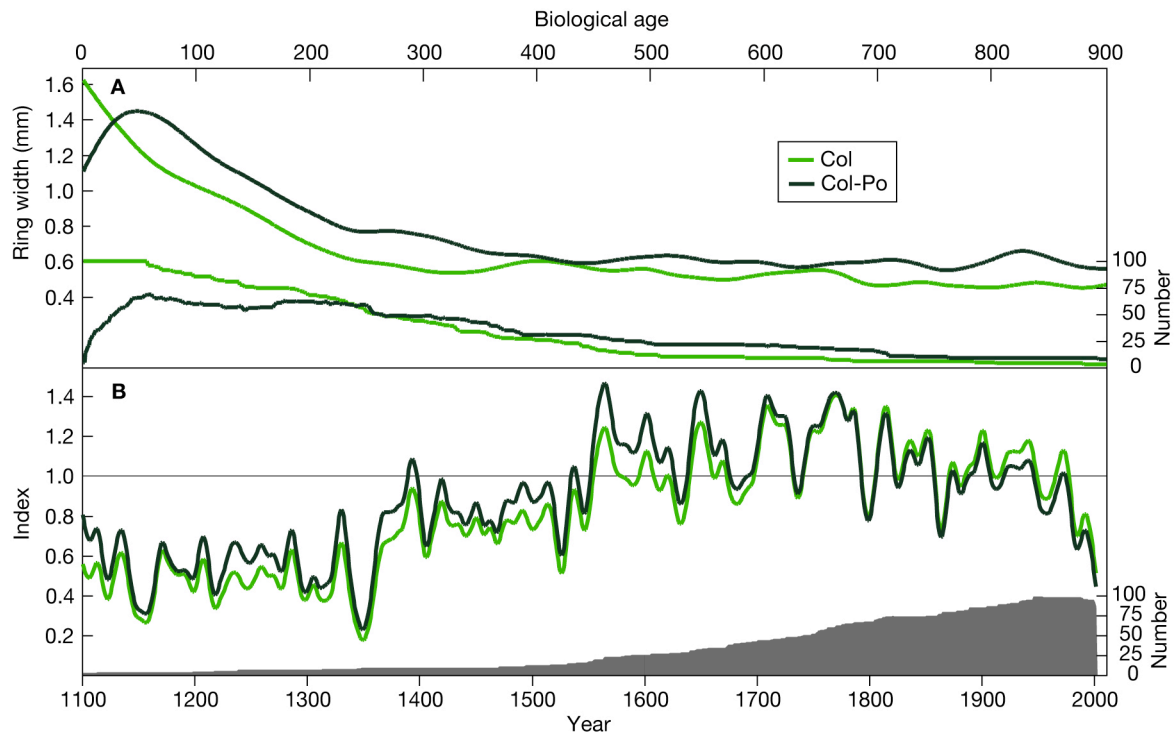


Figure S5. Effect of pith offset within the RCS procedure. **(A)** Regional curves (RC) of the Col and Col-Po data. Replication curves at the bottom of the panel. **(B)** 20-year smoothed RCS chronologies of the Col and Col-Po data. Replication, here sorted by calendar year, is the same for Col and Col-Po (bottom).

To further explore the long-term trend in RCS chronologies, we re-analyzed the largest site dataset (Col) from which we had a complete set of tree diameter measurements. These measurements were utilized to derive a set of PO estimates considering the length of core samples, the curvature of innermost rings on core samples, and the size of trees in sampling height. Consideration of PO results in notable changes of initial growth rates of the age-aligned data in comparison to the data without PO inclusion (Figure S5 A). While these changes were quite sizeable and also in line with expectations [Esper *et al.*, 2003a], the effect on resulting chronologies and particularly on the long-term positive trend over the past millennium is minor (Figure S5 B). Consideration of PO in an old growth cedar site does not significantly alter the low frequency spectrum of RCS chronologies.

4. Combined Norm-RCS record and calibration against February-June PDSI data

For PDSI reconstruction, a combination of the Norm and RCS Old records was used (Figure S6). From the suite of detrendings performed, we suggest that Norm is least likely to possess either tree age or pith offset related biases, as it does not include measurement series shorter than AD 1400 and additionally excludes tree-rings younger than 200 years biological age (the TCTJ-1400 sub-sample). Alignment of tree-rings older than 200 years demonstrated that these data are free of age-related,

biological noise (Figure S6 A). Additionally, these records have been identified as intermediate members representing the center of the low frequency spectra of tree-ring chronologies (see above, Figure S3).

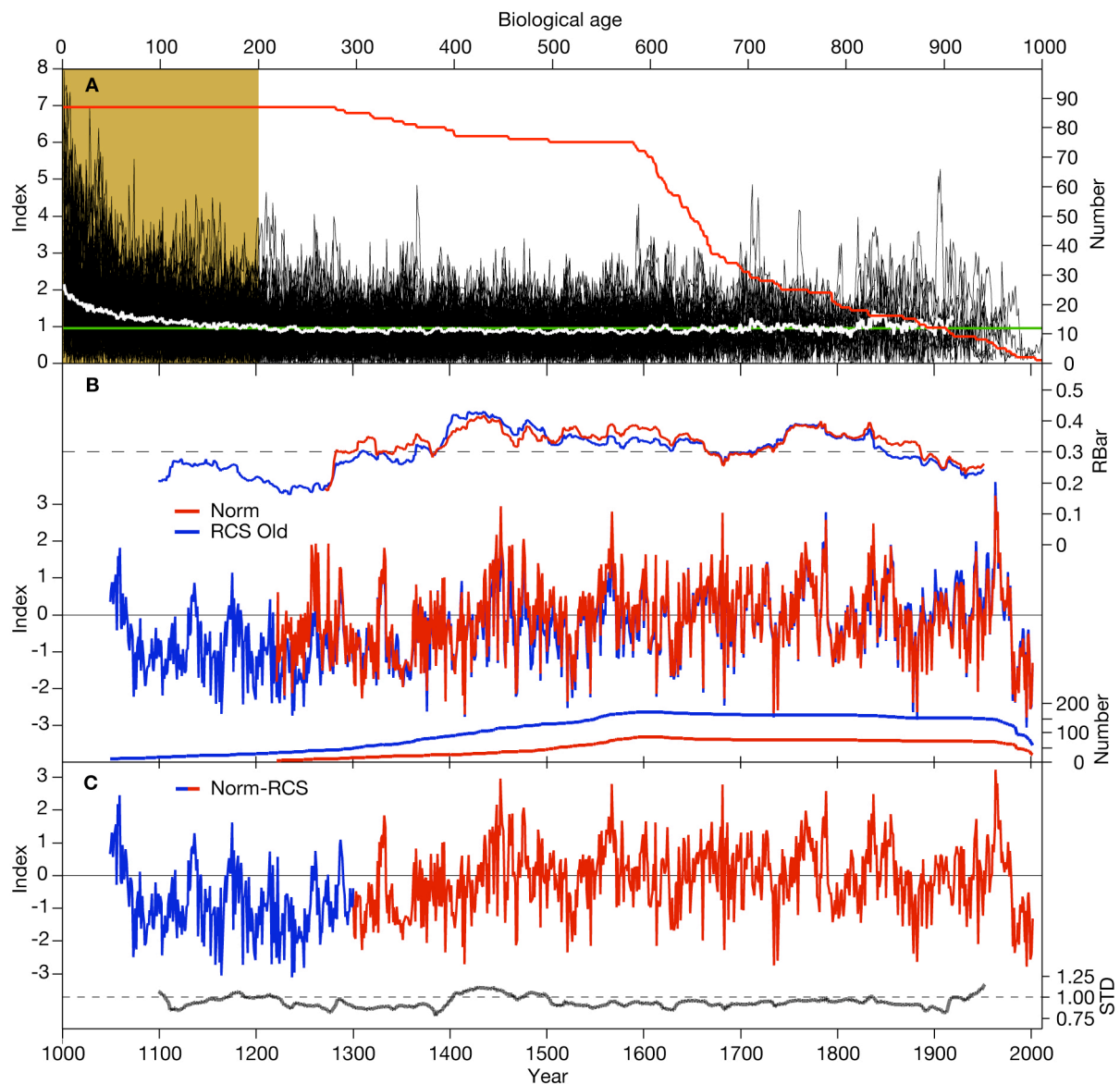


Figure S6. Development and combination of the Norm and RCS Old chronologies. **(A)** 87 individual measurement series (black curves) that meet the requirements for consideration in the Norm chronology (i.e., include rings <AD 1400). Series are normalized and aligned by biological age. White curve is the arithmetic mean, red curve data replication, and green curve the arithmetic mean of the rings 201-220 (0.95). Brown box emphasizes the first 200 years. **(B)** Norm and RCS Old chronologies together with RBar (top) and replication curves (bottom). Norm is truncated at $n = 10$ (AD 1271) and RCS Old at $n = 5$ (AD 1049). Chronologies are normalized over 1600-2001. **(C)** Combined Norm-RCS chronology together with a 100-year running standard deviation curve at the bottom.

A downside of the Norm record, however, is the substantial data reduction in TCTJ-1400, which results in a length restriction to AD 1271 when Norm drops below 10 measurements series (see replication curves in Figure S6 B). The early portion of the past millennium is represented by RCS Old, as this record integrates 40 series in 1271, and 10 series in 1049. The mean and variance of RCS Old were adjusted over the 1300-1350 period to Norm; the combined Norm-RCS record is represented by Norm back to 1300 and by RCS Old prior to this year.

Correlations between Norm and RCS Old over the 1300-1350 and 1300-2001 periods are 0.87 and 0.96, respectively. Comparison of RBar timeseries – which is the average correlation coefficient among all pairs of series combined in a chronology – demonstrated similarity of common variance between Norm and RCS Old (Figure S6 B). The RBar reaches a peak value of about 0.4 during the 15th century and a minimum of about 0.15 in the 13th century. Such variations in RBar may produce variance artifacts [Frank *et al.*, 2007]. Notably, a running standard deviation timeseries of the combined record remains stable over time, and does not possess any obvious systematic shift at the transition between the Norm and RCS records (Figure S6 C).

Verification	R²	RE	CE
1931-1965	0.43	0.63	0.35
1966-2001	0.58	0.67	0.50
Full Period	R²	Res. Reg. Slope	Res. R²
1931-2001	0.56	$y = 0.019x$	0.041

Table S3. Verification statistics of the long-term February-June PDSI reconstruction.

Calibration/verification tests of the linearly regressed Norm-RCS record revealed a temporally robust model explaining 56% of February-June PDSI data over the 1931-2001 period (Table S3). RE and CE statistics suggest skill in the low frequency domain, and the small trend present in model residuals indicates satisfactory agreement between the predictor and predictand. The Durbin Watson statistic (1.1) indicates significant 1st order autocorrelation in the model residuals (Durbin and Watson, 1951). However, this statistic might be of limited use due to the high first order autocorrelation (about 0.7) in the proxy and target data. Verification statistics of the four other, differently detrended chronologies are similar.

Interestingly, the $r = 0.75$ correlation with February-June PDSI data over the 1931-2001 period increases to 0.8 if the first years 1931-1934 are omitted. This decrease in correlation possibly indicates some inhomogeneity in the earliest instrumental measurements. However, without clearer evidence we did not feel it is appropriate to truncate the calibration interval.

5. Uncertainty estimation of the PDSI reconstruction

Three types of error have been identified, including uncertainty arising from (i) the variety of detrending methods that can be chosen for tree-ring standardization and the difficulty of a justified selection of the most suitable method (detrending error), (ii) the temporally changing number and variance of ring width measurement series combined in the mean chronology (chronology error), and (iii) the unexplained variance in the regression model derived from calibration against February-June PDSI data (calibration error).

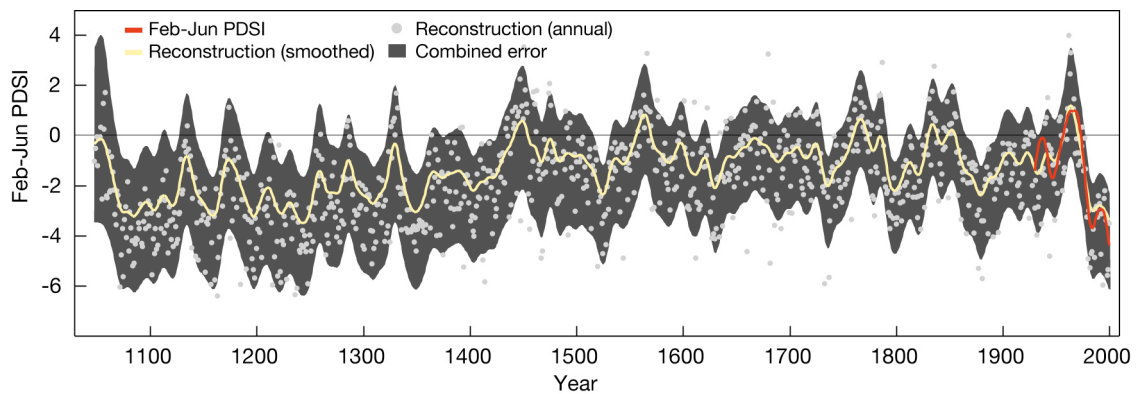


Figure S7. Long-term PDSI reconstruction and uncertainty. 20-year smoothed PDSI reconstruction back to AD 1049 (yellow curve) together with the February-June PDSI target data back to 1931 (red curve). Gray dots indicate annual variability of the reconstruction. Dark band is the combined uncertainty integrating the detrending, data and calibration errors.

(i) Detrending error

Five different detrending methods have been applied using various sub-sets of the combined TCTJ tree-ring data. Resulting mean chronologies were normalized over the 1600-2001 period during which little long-term trend is recorded in any of these records. The range between the maximum and minimum chronology values for each year since AD 1049 is utilized to represent the detrending error. This error effectively signifies the uncertainty in selecting the most appropriate detrending method.

The timeseries representing the upper and lower bounds of the various tree-ring chronologies have been transferred into PDSI estimates using the regression equation derived from Norm-RCS calibration. Discrepancies between the differently detrended tree-ring chronologies are largely restricted to the centennial scale, i.e. the detrending error is essentially a representation of the long-term climatic signal uncertainty in cedar trees. Note that Norm-RCS does not necessarily

fall in the center of the detrending error limits, as it can also represent the highest or lowest values during certain periods (Figure 2).

The detrending error also does not consider more significant deviations that may occur from the utilization of additionally or more questionable methods. For example, many dendroclimatic studies, particularly of moisture stressed trees, have found increases in explained calibration statistics by removing the biological autocorrelation via an autoregressive model. This “detrending” however essentially removes all low-frequency variability. We did not feel that such a step was appropriate given the multi-decadal to centennial scale similarities in the individual measurement series and site chronologies. Thus, we restrict our detrending uncertainties to what we consider a reasonable range of technique. Unfortunately, no objective criterion is possible to determine what should fall within this reasonable range.

(ii) Chronology error

Changes in uncertainty related to the varying number of ring width measurement series back in time and the variance of these series around the mean value function are estimated using bootstrap confidence intervals [Briffa *et al.*, 1992]. In this procedure, the available standardized indices were sampled with replacement 1000 times and arithmetic means calculated. The empirical distribution of these 1000 bootstrap means for each year served as the basis for estimating two-tailed 95% confidence limits. The confidence limits include corrections for bias and skew, which provide second-order correctness.

As with the combined Norm-RCS record, bootstrap intervals were derived back to 1300 from Norm, and between 1049-1299 from RCS Old. Resulting chronology error estimates have been transferred into PDSI estimates using the regression model derived from calibrating Norm-RCS.

(iii) Calibration error

We used two standard error (SE) 95% confidence intervals derived from linear regression of Norm-RCS against instrumental February-June PDSI data to estimate the calibration error. In this procedure, 20-year smoothed tree-ring and PDSI data over the full 1931-2001 calibration period have been considered. We thus illustrate uncertainty based upon the timescale of the reconstruction shown in figure 2. The greater agreement between the tree-ring and PDSI data in the lower-frequency domain is indicated by R^2 values for the original (0.562) and 20-year smoothed (0.903) proxy and instrumental data.

These error terms have been quantified separately (Figure 2) and combined (Figure S7) to allow for an estimation of the overall error of the long-term PDSI reconstruction. The combined uncertainty is represented by the square root of the summed and squared individual errors. While errors (i) and (ii) generally increase back in time, error (iii) remains constant. Consequently, relevance of the calibration error decreases from 64% in the 20th century to 43% over the 1049-1100 period. Whereas the relative

influence of the chronology and detrending errors increases over these periods from 24% to 28% and from 12% to 29%, respectively.

Overall, error estimation of the new reconstruction might appear conservative. However, consideration of three error types likely provides a more comprehensive understanding of the total error associated with tree-ring based reconstructions and their sources. Most typical, only consideration of the error arising from changes in sample replication (type *ii*) or calibration (type *iii*) is provided.

6. Driving synoptic patterns

Temporal variation of the mean geopotential height anomalies as shown in figure 3 was analyzed by comparing the pressure field data [Kistler *et al.*, 2001; Luterbacher *et al.*, 2002] during the second half of the 20th century with the pre-anthropogenic 1659-1900 period (Figure S8). The scaled composites for these time slices indicated that the general circulation patterns – significantly positive geopotential height anomalies in S Europe during dry years, and negative anomalies centered in the eastern Mediterranean area during wet years – remained fairly stable over time.

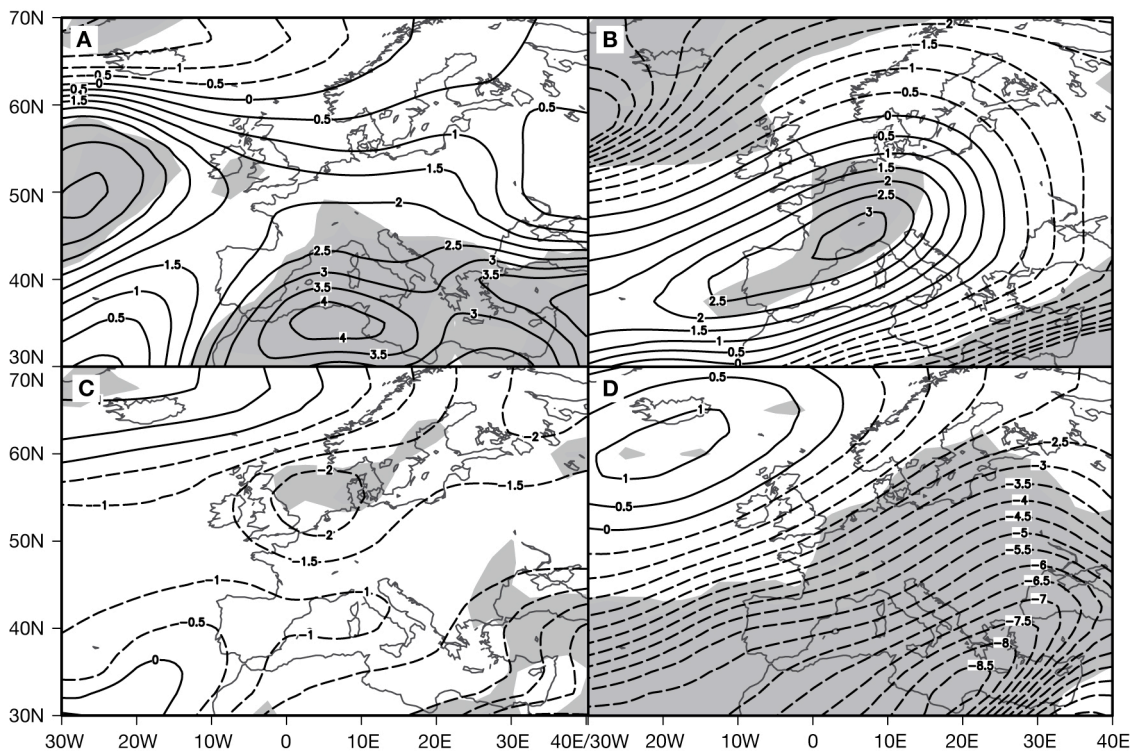


Figure S8. Scaled anomaly composites of the February-June 500 hPa patterns during exceptional dry and wet years in Morocco, over (A) 1948-2001 considering 6 dry years, (B) 1659-1900 considering 9 dry years, (C) 1948-2001 considering 7 wet years, and (D) 1659-1900 considering 25 wet years. Selected years exceed 1.5 standard deviations from the long-term PDSI mean. Significance of identified composite anomaly patterns is

assigned using a modified two-sided t test [Brown and Hall, 1999], with areas where $p < 0.1$ highlighted in gray. Units are arbitrary.

During regionally dry years, the reconstructed PDSI and pressure data also indicate a slight weakening of the Azores high as well as a minor NE shift of the maximum mid troposphere pressure center towards S France in comparison to the modern period. In combination with this shift, we found a steeper pressure gradient towards the E Mediterranean area during historical times in comparison to the 20th century data (Figures S8 A-B). Circulation pattern detection also revealed lower pressure anomalies and steeper gradients during the 1659-1900 period for Moroccan wet years. While this historically intensified pattern also affected the spatial domain over which pressure deviations are statistically significant (gray area in Figures S8 C-D), the overall synoptic situation, as indicated by negative deviations in the SE sector and positive deviations in NW sector, remained effectively the same and consistent with pressure and circulation patterns expected during wet and dry years.

7. Comparison with gridded PDSI proxy

Comparison of the long-term February-June PDSI record with a gridded annual PDSI reconstruction, derived from a multitude of proxy data including Moroccan cedar trees [Guiot *et al.*, 2005], revealed high correlation (0.75) for the post-1931 calibration period, but no correlation for the pre-1931 period back to 1350 (Figure S9). The excellent 20th century fit is somehow not surprising though, as the gridded reconstruction correlates at >0.9 against local instrumental PDSI data.

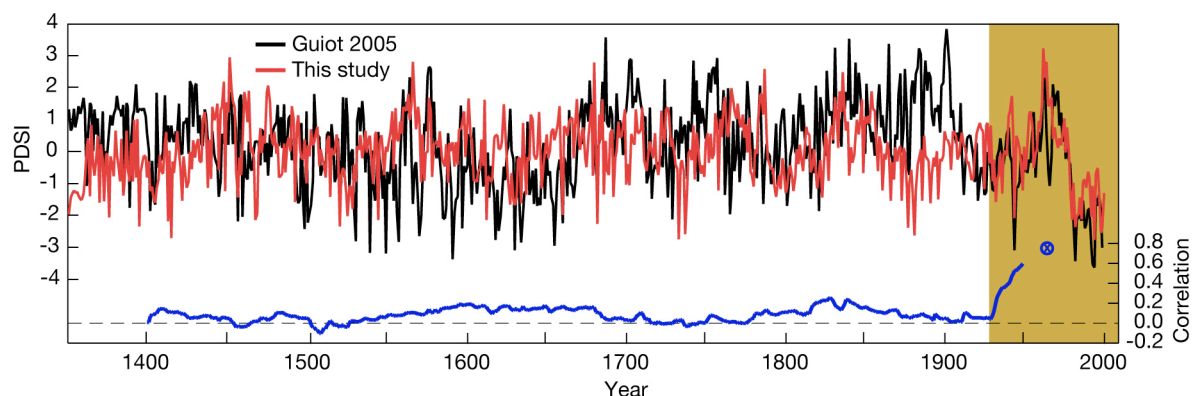


Figure S9. Comparison of the long-term PDSI reconstruction with the record from Guiot *et al.* (2005) for grid point N32.5/E-5. Blue curve indicates moving 100-year correlations, and blue dot the correlation over the 1931-2000 calibration period (emphasized with the brown box).

The lack of coherence before 1931, however, suggests overfitting of the neural network based calibration model used by *Guiot et al.* [2005]. This conclusion is drawn as the loss of skill appeared exactly at the transition between the training and reconstruction periods. Interestingly, the *Guiot et al.* [2005] reconstruction includes longer term Moroccan tree-ring data. Our analysis of these data revealed temporally robust coherence between cedar site chronologies (Figure S1, Table S2), as well as between young and old tree-rings over the past 400 years (Figure S4), indicating spatial and temporal consistency in the long-term PDSI reconstruction. Moreover, comparison with mid troposphere pressure field reconstructions (Figures 3 and S8) showed that the larger-scale circulation patterns indicative of regionally dry and wet years, remained unchanged over the past 350 years. All these results indicate the PDSI signal in the present study to be stable over longer timescales.

References

- Briffa, K. R., P. D. Jones, T. S. Bartholin, D. Eckstein, F. H. Schweingruber, W. Karlén, P. Zetterberg, and M. Eronen (1992), Fennoscandian summers from AD 500 – temperature-changes on short and long timescales, *Clim. Dyn.*, 7, 111-119.
- Cook, E. R., J. Esper, R. D'Arrigo (2004), Extra-tropical Northern Hemisphere temperature variability over the past 1000 years, *Quat. Sc. Rev.*, 23, 2063-2074.
- Durbin, J, and G. S. Watson (1951), Testing for serial correlation in least squares regression. *Biometrika*, 38, 159-78.
- Esper, J., E. R. Cook, P. J. Krusic, K. Peters, and F. H. Schweingruber (2003a), Tests of the RCS method for preserving low-frequency variability in long tree-ring chronologies, *Tree-Ring Res.*, 59, 81-98.
- Esper J., S. G. Shiyatov, V. S. Mazepa, R. J. S. Wilson, D. A. Graybill, and G. Funkhouser (2003b), Temperature-sensitive Tien Shan tree ring chronologies show multi-centennial growth trends, *Clim. Dyn.*, 8, 699-706.
- Esper, J. D. C., and R. J. S. Wilson (2004), Climate reconstructions - low frequency ambition and high frequency ratification, *EOS*, 85, 113, 120.
- Esper, J., U. Büntgen, D. C. Frank, D. Nievergelt, K. Treydte, and A. Verstege (2006), Multiple tree-ring parameters from Atlas cedar (Morocco) and their climatic signal, in *Tree rings in archaeology, climatology and ecology*, edited by I. Heinrich et al., pp. 46-55, Reihe Umwelt/Environment, 61, Jülich.
- Esper J., D. C. Frank, and J. Luterbacher (2007a), On selected issues and challenges in dendroclimatology, in *A changing world: challenges for landscape research*, edited by F. Kienast et al., pp. 113-132, Springer, Berlin.

- Esper, J., D. C. Frank, R. J. S. Wilson, U. Büntgen, and K. Treydte (2007b), Uniform growth trends among central Asian low and high elevation juniper tree sites. *Trees*, *21*, 141–150.
- Frank, D. C., J. Esper, and E. R. Cook (2007), Correction for proxy number and coherence in a large-scale temperature reconstruction, *Geophys. Res. Lett.*, in press.
- Guiot, J., S. Alleaume, A. Nicault, and S. Brewer (2005), The Mediterranean droughts during the last 650 years: reconstruction from tree-rings and climate model simulation. *Geophys. Res. Abstracts*, *7*, 02471, European Geoscience Union, Vienna, 24-29 April 2005.
- Kistler, R., et al. (2001), The NCEP-NCAR 50-year Reanalysis: monthly means CD-ROM and documentation. *Bull. Am. Meteorol. Soc.*, *82*, 247-267.
- Luterbacher, J., E. Xoplaki, D. Dietrich, R. Rickli, J. Jacobeit, C. Beck, D. Gyalistras, C. Schmutz, and H. Wanner, (2002), Reconstruction of Sea-Level Pressure Fields over the Eastern North Atlantic and Europe Back to 1500, *Clim. Dyn.*, *18*, 545-561.
- Mann, M. E., and J. M. Lees (1996), Robust estimation of background noise and signal detection in climatic time series, *Clim. Change*, *33*, 409–445.
- Wigley, T. M. L., K. R. Briffa, and P. D. Jones (1984), On the average of correlated time series, with applications in dendroclimatology and hydrometeorology, *J. Clim. Appl. Meteorol.*, *23*, 201-213.